Organic Geochemistry 71 (2014) 17–29

Contents lists available at ScienceDirect

Organic Geochemistry

journal homepage: www.elsevier.com/locate/orggeochem

The effect of oil expulsion or retention on further thermal degradation of kerogen at the high maturity stage: A pyrolysis study of type II kerogen from Pingliang shale, China

Wanglu Jia [a], Qiuling Wang [a], Jinzhong Liu [a], Ping'an Peng [a,*], Baohua Li [b], Jialan Lu [a]

[a] State Key Laboratory of Organic Geochemistry, Guangzhou Institute of Geochemistry, Chinese Academy of Sciences, Guangzhou 510640, China
[b] Tarim Oilfield Company, PetroChina, Kuerle 841000, China

ARTICLE INFO

Article history:
Received 29 August 2013
Received in revised form 23 February 2014
Accepted 23 March 2014
Available online 1 April 2014

Keywords:
Oil expulsion or retention
Hydrocarbon generation
High maturity stage
Oil and gas composition
Isotopic signature

ABSTRACT

High maturity oil and gas are usually generated after primary oil expulsion from source rocks, especially from oil prone type I/II kerogen. However, the detailed impacts of oil expulsion, or retention in source rock on further thermal degradation of kerogen at the high maturity stage remain unknown. In the present study, we collected an Ordovician Pingliang shale sample containing type II kerogen. The kerogens, which had previously generated and expelled oil and those which had not, were prepared and pyrolyzed in a closed system, to observe oil expulsion or oil retention effects on later oil and gas generation from kerogen. The results show that oil expulsion and retention strongly impacts on further oil and gas generation in terms of both the amount and composition in the high maturity stage. Gas production will be reduced by 50% when the expulsion coefficient reaches 58%, and gas from oil-expelled kerogen (less oil retained) is much drier than that from fresh kerogen. The oil expulsion also causes *n*-alkanes and gas compounds to have heavier carbon isotopic compositions at high maturity stages. The enrichment of ^{13}C in *n*-alkanes and gas hydrocarbons are 1‰ and 4–6‰ respectively, compared to fresh kerogen. Oil expulsion may act as open system opposite to the oil retention that influences the data pattern in cross-plots of $\delta^{13}C_2-\delta^{13}C_3$ versus C_2/C_3, $\delta^{13}C_2-\delta^{13}C_3$ versus $\delta^{13}C_1$ and $\delta^{13}C_1-\delta^{13}C_2$ versus $\ln(C_1/C_2)$, which are widely used for identification of gas from kerogen cracking or oil cracking. These results suggest that the reserve estimation and gas/source correlation in deep burial basins should consider the proportion of oil retention to oil expulsion the source rocks have experienced.

1. Introduction

Oil expulsion, during which the oil produced from the thermal degradation of kerogen moves out from the kerogen structure and migrates into the rock matrix, is the first step in the primary migration of oil in the source beds (Tissot and Welte, 1984; Pepper and Corvi, 1995; Kelemen et al., 2006a). During the maturing process, the adsorption of generated oil onto the kerogen (retention) and the diffusion of oil through the kerogen are believed to control the oil expulsion (Thomas and Clouse, 1990; Pepper and Corvi, 1995), and the solubility of organic compounds in the kerogen could well account for the compositional differences between the expelled oil and retained bitumen (Sandvik et al., 1992; Ritter, 2003; Ertas et al., 2006; Kelemen et al., 2006a,b). Calculations based on the swelling theory and experimental data have shown that oil expulsion efficiencies of type I and II kerogen could be very high (from 40–90%), and vary with hydrocarbon generation potentials (type of organic matter), maturity and compositions of generated oils (Sandvik et al., 1992; Ritter, 2003; Kelemen et al., 2006b; Wei et al., 2012). The high oil expulsion efficiencies for type I and type II kerogen in the oil window were also validated by geological section studies in the Ordos Basin (Zhang et al., 2006) and Bohai Bay Basin (Pang et al., 2005). Meanwhile, the transformation ratio of oil from type I and II kerogen may reach 60% or more, as evidenced by many laboratory and field observations (Andresen et al., 1995; Pepper and Corvi, 1995; Behar et al., 1997; Lewan, 1997; Xiong et al., 2002; Pan et al., 2010; Lewan and Roy, 2011; Wei et al., 2012). The high transformation ratio, in conjunction with high expulsion efficiency, allows substantial kerogen mass loss during the oil expulsion. For example, kerogen may lose half of its mass if the transformation ratio and expulsion efficiencies are 60% and 90%, respectively. The loss of kerogen mass

* Corresponding author. Address: Guangzhou Institute of Geochemistry, Chinese Academy of Sciences, 511 Kehua Street, Guangzhou 510640, China. Tel.: +86 20 85290126; fax: +86 20 85290117.
E-mail address: pinganp@gig.ac.cn (P. Peng).

http://dx.doi.org/10.1016/j.orggeochem.2014.03.009
0146-6380/

may have a series of effects on subsequent oil and gas generation of kerogen residue, not only affecting the amount but also the chemical and isotopic composition.

High maturity crude oil (e.g., Chen et al., 1996; Hao et al., 1996; Carrigan et al., 1998; Sajgó, 2000; Zhou et al., 2003; Zhang et al., 2005) and gas (e.g. Lorant et al., 1998; Lorant and Behar, 2002; Hill et al., 2007; Rodriguez and Philp, 2010; Tian et al., 2010; Hao and Zou, 2013; Xia et al., 2013) occurring in many deep-burial basins may be derived from the thermal degradation of kerogen which has experienced oil expulsion. Opposite to oil expulsion, oil retention in source rock could impact the resource potential of shale oil and gas; hot exploration targets in recent years. It is of scientific importance to characterize the hydrocarbon generation behavior of oil-expelled kerogen, because it may help us to precisely estimate conventional and unconventional oil/gas reserves and perform source to oil/gas correlation in deep-burial basins. The best approach for this study is to pyrolyze a kerogen, and characterize the oil generation and expulsion from natural or artificially mature samples (Lorant and Behar, 2002; Hill et al., 2007; Guo et al., 2009; Tian et al., 2010).

The variations in both carbon and hydrogen isotopic compositions of kerogen or oil during maturation have been well studied by laboratory thermal simulation (Lewan, 1983; Clayton, 1991; Bjorøy et al., 1992; Schimmelmann et al., 1999; Tang et al., 2005). Oil fractions are expected to be increasingly enriched in ^{13}C and D in the order asphaltenes > resins > aromatics > saturates (Stahl, 1978), although carbon isotopic compositions of oil fractions in natural samples could display more complicated variations (Fekete et al., 2009). The oil expulsion process generally leaves residual bitumen in the kerogen with more NSO compounds than in the expelled oils and aromatics are more retained in kerogen than the saturates (Sandvik et al., 1992; Ritter, 2003; Kelemen et al., 2006a). Therefore, the kerogen that has experienced oil expulsion will be enriched in ^{13}C and D relative to fresh kerogen that has not expelled oil. Theoretically, the gas and oil generated by oil-expelled kerogen could be more enriched in ^{13}C than that generated by fresh kerogen. However, the exact differences in $\delta^{13}C$ and δD of pyrolysates between oil-expelled and fresh kerogen are not known and need to be determined experimentally.

In the present study, an oil-expelled type II kerogen (KAE) was artificially prepared. Both KAE and fresh kerogen (KO) were subjected to a thermal degradation simulation in a closed system. The amount, and molecular and carbon isotopic compositions, of generated gases and liquid hydrocarbons were determined and compared. The residual solids after thermal degradation were also analyzed to provide insights for the effects of oil expulsion or retention on the hydrocarbon generation of type II kerogen in high to overmature stages. The kinetic and compositional data reported in this paper are useful for estimates of conventional and unconventional oil and gas reserves and for source to oil/gas correlation in deep-burial basins.

2. Samples and methods

2.1. Samples

Pingliang black shale, a Middle-Upper Ordovician marine source rock, was collected from an outcrop in the Ordos Basin. The shale contains total organic carbon (TOC) of 18.1% with S1 3.2 mg/g, S2 65.1 mg/g, S3 0.5 mg/g, HI 360 mg HC/g TOC, OI 3 mg CO_2/g TOC, Tmax 434 °C and bitumen reflectance 0.7% (BRo). The rock is marginally mature and contains type II kerogen. The rock sample was crushed and pulverized to less than 200 mesh. The kerogens were prepared by a standard procedure in which the rock powder was treated with hydrofluoric and hydrochloric acids. The isolated kerogen had an atomic H/C ratio of 1.76 and $\delta^{13}C$ value of −30.1‰.

2.2. Experimental method

2.2.1. The preparation of oil-expelled kerogen (KAE)

A stainless steel vessel (3 cm o.d., 1.2 cm i.d., Fig. S1), equipped with a seal unit at each end, was used to prepare the oil-expelled kerogen. First, one end of the pre-cleaned vessel was tightly connected with a seal unit, and some powdered muddy sandstone (heated at 450 °C for 5 h after solvent extraction) was loaded into the vessel and then compacted by a jack under a pressure of 40 MPa. Second, the isolated kerogen was loaded in the middle of the vessel in the same way as the sandstone and then another sandstone section was loaded. Finally, the other end of the vessel was capped with a seal unit. In this system, the two end parts of the vessel were filled with sandstone to provide space for any oil expelled from the kerogen. The vessel was heated in an oven at 330 °C for 72 h (mature to a BRo of 1.0%). After cooling, one seal unit was slowly opened to allow the generated gas to be progressively released into the air, and then the other seal unit was removed. The mixture column, the kerogen section and two sandstone sections, was pushed out of the stainless vessel, which was also facilitated by the jack. The mature kerogen KAE was carefully separated from the sandstone. The recovered mature kerogen, including residual bitumen, was used directly in the subsequent pyrolysis experiment. The sandstone was Soxhlet extracted with dichloromethane:methanol (93:7 v:v) for 72 h, and the extracts were quantified by weight as the expelled oil.

2.2.2. Thermal degradation of kerogens

There are many simulation systems for thermal degradation of kerogen. The model of constant temperature is more applicable to study time effect on the pyrolysis of kerogen, while programmed temperature model suits the investigation of temperature effect. To understand secondary hydrocarbon generation at the high maturity stage, the temperature effect is more important. Thus, we chose a programmed temperature model in this study. The presence of water in the simulation system could also affect the hydrocarbon generation of source rocks containing type I and II kerogen (Lewan, 1997; Lewan and Roy, 2011), which might result in different variations in the kerogen structure in the maturation and oil expulsion efficiencies. At the high maturity stage, water may be not so important as that in the oil window. Therefore, we performed an anhydrous pyrolysis of kerogens in this study. Both KAE and KO were pyrolyzed in sealed gold tubes. The detailed procedure was described by Liu and Tang (1998). Briefly, about 20–80 mg kerogen samples were introduced into gold tubes and the tubes were sealed under argon. Two tubes containing the KAE and KO were loaded into the same stainless vessel. Pyrolysis was performed under a constant pressure of 50 MPa, and the pyrolysis temperatures ranged from 250–600 °C at heating rates of 20 °C/h and 2 °C/h.

2.3. Analysis

2.3.1. Molecular and carbon isotopic compositions of generated gas

Analytical procedures follow those reported by Pan et al. (2006). The gold tube was carefully loaded into a customized vacuum line connected with an Agilent 6890N GC modified by Wasson ECE Instrumentation for determination of gas molecular composition. Next, the system was evacuated by a rotary pump and the gold tube was pierced to allow the gas flow into the vacuum line. A valve lies between the vacuum line and the GC instrument was used to automatically introduce a certain amount of gas into the GC system for measurements of molecular composition. After the GC analysis, a gas-tight syringe was used to extract the remaining gas from the vacuum line for the carbon isotope analysis. Carbon isotope analysis of the gas components was performed using a

GV Isoprime IRMS interfaced with an Agilent 6980 GC. Each sample was measured in two runs and the average for the two runs was accepted as the final sample isotopic composition. The precision of the isotopic analysis was generally better than 0.4‰ for carbon isotopic composition. Gas with a pre-determined $\delta^{13}C$ value was analyzed regularly to check the accuracy of the measurement.

2.3.2. Analysis of the generated liquid hydrocarbons

After analysis of the gas hydrocarbons, the gold tube was opened and ultrasonically extracted with dichloromethane, and a known amount of C_{24} deuterated *n*-alkane was added into the solution. The solution of total extracts was directly analyzed on an Agilent 6890 GC equipped with an FID to determine the amounts of released *n*-alkanes. Then, the extracts were filtered and were subject to column chromatography on silica gel (80–100 mesh)/Al_2O_3 (100–200 mesh). The saturated and aromatic fractions were eluted with *n*-hexane and *n*-hexane:dichloromethane (2:1 v:v), respectively. They were analyzed using a Thermo DSQ MS coupled to a Trace GC for determination of biological markers.

A parallel suite of gold tubes without any treatment was directly opened and ultrasonically extracted with dichloromethane, and the extracts were filtered. The filtrate, i.e. liquid hydrocarbon, was dried and weighed. The liquid hydrocarbon was further separated into saturates and aromatics by column chromatography on silica gel/Al_2O_3. The saturates were then purified by urea adduction to obtain the *n*-alkane fractions, and compound specific carbon isotopic analysis was performed on a GV Isoprime IRMS instrument interfaced with a HP6890 GC via a combustion interface. Hydrogen isotopic analysis was performed on a Finnigan Delta$^+$ XL IRMS interfaced with a HP6890 GC via a high temperature conversion interface. A mixture of *n*-alkane standards (provided by Dr. A. Schimmelmann of Indiana University) was measured to monitor the GC-IRMS system. Each sample was analyzed in duplicate, and the average for the two runs was accepted as the final sample isotopic composition. The precision was generally better than 0.5‰ and 5‰ for carbon and hydrogen isotopes, respectively.

2.3.3. Analysis of residual solids after the pyrolysis

The solids remaining in the gold tube after extraction were dried. The total carbon isotopic compositions were measured on a Finnigan Delta$^+$ XL IRMS instrument coupled to a CE flash1112 EA via a ConfloIII interface. A working standard (black carbon) was measured to monitor the EA-IRMS system. Generally, each sample was analyzed in duplicate and the average for the two runs was accepted as the final sample isotopic composition. The precision of the total carbon isotope analysis was usually better than 0.2‰. Six samples have been analyzed in triplicate in this work, and SD (standard deviation) of the triplicate analysis is generally < 0.1‰. The solids were also analyzed by Vinci Rock–Eval 6 to obtain the data such as HI and Tmax.

3. Results and discussion

According to the resulting weights of expelled oils and residual bitumen (34.9 and 25.4 mg/g kerogen KO, respectively), about 58% of the total liquid hydrocarbons generated were expelled in this experiment.

3.1. Compositions of residual solids and generated hydrocarbons

3.1.1. Residual solids

Because the residual solids were extracted with dichloromethane, only the HI and Tmax data from the Rock–Eval analysis are meaningful when considering the chemical structure of kerogen under pyrolysis (Fig. 1). As expected, the HI of residual solids of both KAE and KO decreased progressively with increasing temperatures. The effects of oil generation and expulsion on HI and Tmax were apparent, in that the HI of residual solids from KO decreased more rapidly than that from KAE. The HI of residual solids from KAE was significantly lower than that of KO at the pyrolysis temperature < 384 °C, since kerogen KAE has generated oil at a BRo of 1.0%. For the same reason, the Tmax of residual solids of KAE remained at high levels even when the pyrolysis temperatures were relatively low (< 384 °C). The Tmax of residual solids of KO increased significantly from 440–580 °C when the pyrolysis temperature increased from 360–384 °C, and the Tmax of residual solids of KAE approached that of KO at the pyrolysis temperature of 384 °C. Moreover, the HI of residual solids of both KO and KAE decreased to ~10 mg/g TOC when the pyrolysis temperature reached 384 °C. The Tmax values of residual solids of KO and KAE were similar when the pyrolysis temperature was > 384 °C, which indicates that Tmax is only weakly influenced by oil expulsion at the high maturity stage. Relatively lower HI in residual solids of KO compared to that in the residual solids of KAE at the pyrolysis temperature of 384 °C could be explained by the reduced formation of pyrobitumen due to the oil expulsion. Pyrobitumen is mainly derived from aromatic condensation of oil or bitumen (Ungerer et al., 1988; Behar et al., 1992; Schenk et al., 1997; Hill et al., 2003).

3.1.2. Liquid hydrocarbons

With increasing pyrolysis temperature, the total yields of liquid hydrocarbons (Fig. 2a) and total yields of *n*-alkanes (Fig. 2b) from kerogen KO firstly increased but then decreased. Secondary cracking of generated liquid hydrocarbons and *n*-alkanes, as evidenced by rapid decrease of the total yields, might be significant at the pyrolysis temperatures higher than 360 °C and 384 °C, respectively (Fig. 2a and b). The amounts of extracted bitumens generated by Type II kerogen of the Kimmeridge Formation were reported to decrease at the Ro of 0.8% under hydrous pyrolysis (Andresen et al., 1995), while those generated by the type II kerogen in this work started to decrease at the EasyRo value of 0.9%. The oil generation of type II Toarcian kerogen peaked at the EasyRo value of 1.2% (Dieckmann et al., 1998), and the extracted oil included not

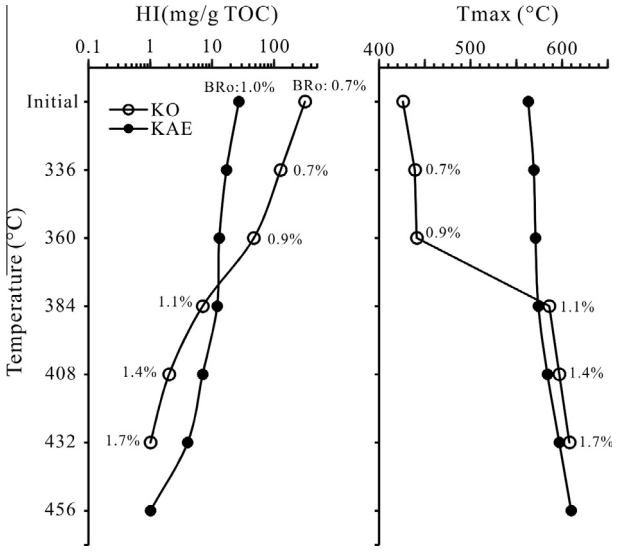

Fig. 1. Rock–Eval data of the residual kerogens after pyrolysis (2 °C/h). Numbers adjacent to the symbols in this and the following figures indicate the EasyRo values, calculated at the heating rate of 2 °C/h using the model by Sweeney and Burnham (1990).

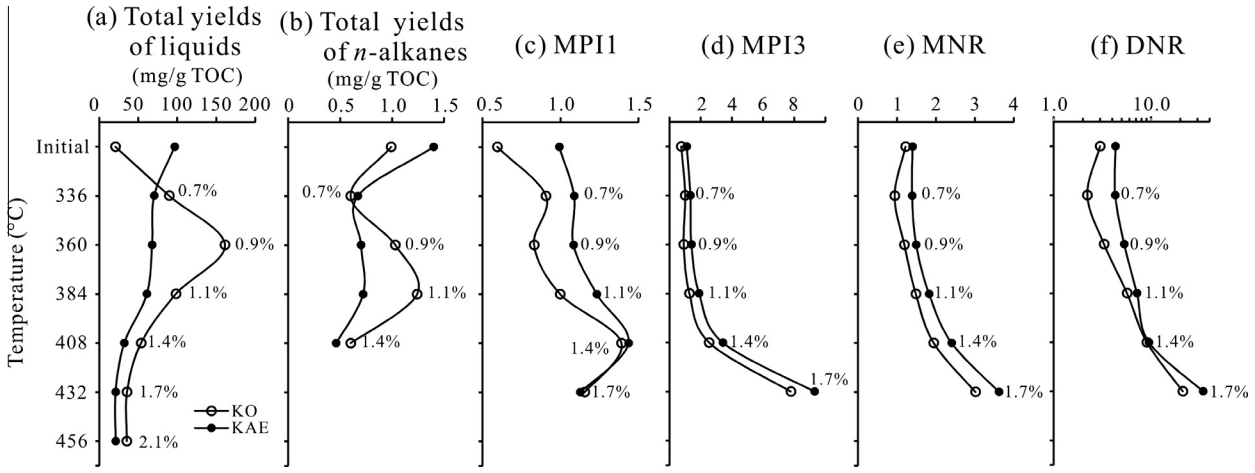

Fig. 2. Yields of liquid hydrocarbons and related maturity indices in the pyrolysis (2 °C/h) of KAE and KO kerogens. MPI1 = 1.5 × (2-MP + 3-MP)/(P + 1-MP + 9-MP), MPI3 = (2-MP + 3-MP)/(1-MP + 9-MP), MNR = 2-MN/1-MN, DNR = (2,6-DMN + 2,7-DMN)/1,5-DMN. Maturity indices were calculated from the mass chromatograms of GC–MS analysis. The initial values were derived from the whole rock extracts (KO series) and expelled oils (KAE series), respectively.

only the C_{15+} fraction but also the C_{6-14} fraction. The secondary cracking of the C_{15+} fraction starts at lower pyrolysis temperatures than that of the C_{6-14} fraction (Dieckmann et al., 1998; Hill et al., 2003; Walters et al., 2007). For example, in the pyrolysis experiments performed under closed conditions at a heating rate of 5 °C/min, secondary cracking of the C_{15+} fraction could occur at temperature ~40 °C lower than cracking of the C_{6-14} fraction (Dieckmann et al., 1998). The total yields of liquid hydrocarbons and total yields of *n*-alkanes generated by KAE were almost the same below the pyrolysis temperature of 384 °C, which may suggest that little new oil was generated from KAE except residual bitumens. This result agrees well with the Tmax and HI data of the residual solids (Fig. 1), which indicates that the KAE had already passed the main oil generation stage. The effects of oil expulsion on the amount of liquid hydrocarbons obtained at high maturity are also consistent with the slightly lower yields of liquid hydrocarbons from KAE relative to those from KO when the pyrolysis temperature was higher than 384 °C (Fig. 2).

Four maturity indices, calculated based on the relative amounts of polycyclic aromatic hydrocarbons generated by KO, increased progressively with increasing pyrolysis temperatures except MPI1 at 408 °C. In contrast, those indices from the KAE varied little below the pyrolysis temperature of 384 °C and then increased (Fig. 2). This result further proves that the KAE had undergone the main oil generation stage. The MPI3, MNR and DNR might be less influenced by the oil expulsion as evidenced by the higher values of these ratios for the KAE relative to those for KO when the pyrolysis temperature was higher than 384 °C. Although no molecular fractionations of aromatic hydrocarbons were observed between expelled oil and retained bitumen in the primary migration (Leythaeuser et al., 1988; Eseme et al., 2007), the data reported in their work suggest that the maturity indices would have been lower if the simulation system was more closed. Notably, a reversal trend as displayed by MPI1 from both kerogen KAE and KO beyond the pyrolysis temperature of 408 °C (EasyRo value of 1.4%) is consistent with the observations from geological samples at Ro values greater than 1.35% (Radke and Welte, 1983).

Although 58% of the oil was expelled from KAE, the bitumen retained by this kerogen (42% of total liquid hydrocarbon) shows a similar composition to that of the liquid hydrocarbons generated by KO in the pyrolysis (Fig. 3). Nevertheless, some notable differences could still be observed between the liquid hydrocarbons generated by the two kerogen samples. The relative amounts of aromatic hydrocarbons generated by KO progressively increased with increasing temperature (Fig. 3a–e). However, the aromatic hydrocarbons generated from KAE varied little in the pyrolysis temperature range 336–384 °C (Figs. 3h–j and 4), which could suggest that no significant pyrolysis reactions occurred in the residual bitumen and kerogen KAE over this temperature range. When the pyrolysis temperature was raised to 408 °C, a significant increase in the relative amounts of aromatic hydrocarbons was observed for both KO and KAE; after further increasing the pyrolysis temperature to 432 °C, few *n*-alkanes were detected (Figs. 3 and 4). The higher stabilities of aromatic hydrocarbons relative to those of saturated hydrocarbons in the simulation experiments have been well documented for the pyrolysis of oils in a closed system (Behar et al., 1999; Hill et al., 2003; Tang et al., 2005), even though the opposite trend has been observed in natural conditions (Horsfield et al., 1992). It is notable that the relative amounts of aromatic hydrocarbons in expelled oils are lower than those generated by KAE in the temperature range from 336–384 °C (Fig. 3g–j, and also evident in the lower ratios of N/*n*-C_{12} and C_2N/*n*-C_{14} for expelled oils, Fig. 4). This result may indicate that saturated hydrocarbons are more easily expelled from the kerogen structure in comparison with aromatic hydrocarbons (Sandvik et al., 1992; Ritter, 2003; Ertas et al., 2006). Terpanes and steranes were relatively abundant in the extracts from the whole rock sample and as pyrolysis temperature increased, the relative amounts of steranes and hopanes decreased rapidly (Fig. S1). Meanwhile, the relative amounts of tricyclic terpanes and Ts increased. However, when the pyrolysis temperature was > 360 °C, few biomarkers were detected either due to relatively low amounts or due to significant secondary cracking at high pyrolysis temperatures. Pyrolysis of type II kerogen from Woodford shale also shows no detection of terpanes and steranes in the pyrolysates when the measured Ro value of residual kerogens was > 1.0% (Lewan, 1997).

3.1.3. Gas hydrocarbons

After oil expulsion, gas yields from KAE were much lower than those from KO because of the reduced contribution from secondary cracking of generated oils (Fig. 5a). The loss of wet gas components during the oil expulsion also played an important role because significant amounts of wet gas components had been generated with EasyRo values from 0.9–1.1% (Fig. 5d and f). More importantly, the relative amounts of C_{1-5} gas were also influenced by the oil expulsion. The amounts of methane, ethane and propane generated by the KAE were about one half, one third and one quarter of those generated by the KO (Fig. 5a–c), respectively. Accordingly, the

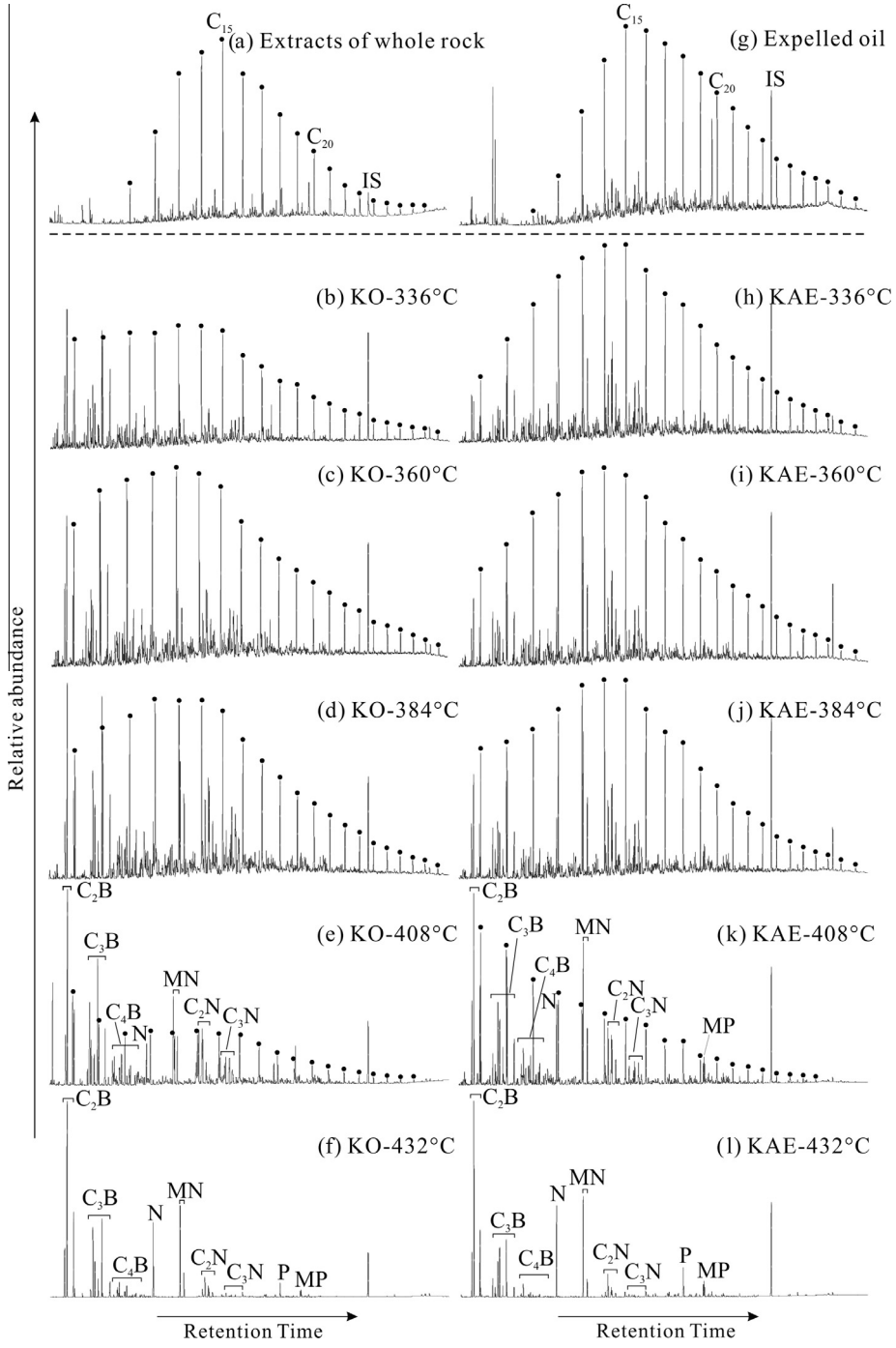

Fig. 3. GC chromatograms of the pyrolysates from KO and KAE at different temperatures (2 °C/h). Black dots indicate normal alkanes produced in the pyrolysis; C_2B, C_3B and C_4B denote C_2-, C_3- and C_4-benzenes; N, naphthalene; MN, C_2N and C_3N denote methyl, C_2-and C_3-naphthalene; P, phenanthrene; MP, methylphenanthrene; IS, internal standards.

gas generated by KAE in the closed system was much drier than gas generated by KO, in the high to overmature stages. These results have been well documented in mature kerogen by many previous studies (Behar et al., 1995, 1997; Hill et al., 2007; Tian et al., 2010). Various types of cleavage reactions may occur in the cracking of oil and mature kerogen; the former is mainly characterized by the cleavage of straight carbon links while the latter mainly involves demethylation or dealkylation reactions (Behar et al., 1999; Lorant et al., 2000). Therefore, after the oil expulsion, the wet gas components generated by KAE (mainly derived from the secondary cracking of residual bitumens) would be much lower than those generated by KO.

The process of gas generation from KAE and KO could be divided into three stages according to variations in the relative amounts of produced gases (Fig. 5f). First was the main generation stage of C_{2-5} with EasyRo values ranging from 0.7% to ~1.4% or higher; in this stage < 20% of total methane and > 70% of total C_{2-5} were formed. Second was the secondary cracking of C_{2-5} with EasyRo values ranging from ~1.7% to ~3.0%, the generation rate of methane increased rapidly and more than 70% of the total methane was accumulated, while < 10% C_{2-5} remained. Third, small amounts of methane (< 20% of the total methane) were generated, with EasyRo values > 3.0%. The similarity between the gas generation pattern of KO and that of KAE suggests that secondary cracking

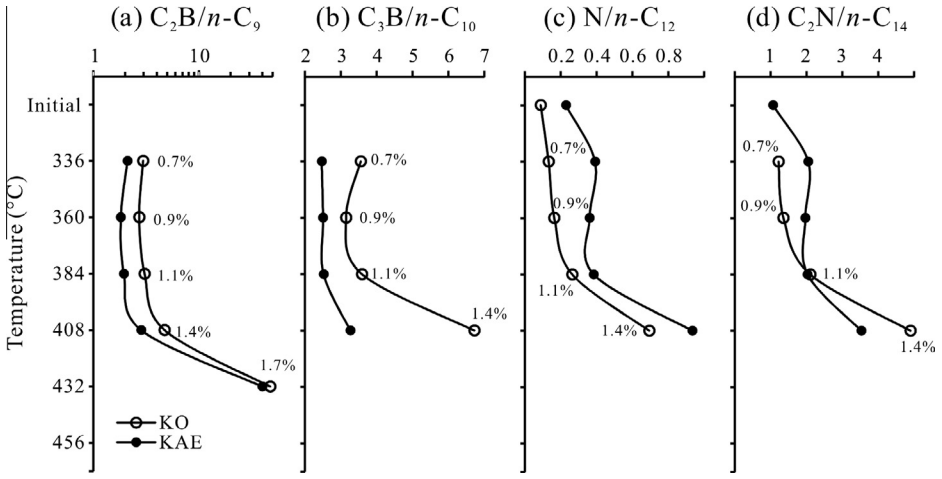

Fig. 4. Variations in molecular ratios with increasing temperatures in the pyrolysis of two kerogen samples (2 °C/h). $C_2B/n\text{-}C_9$, $C_3B/n\text{-}C_{10}$, $N/n\text{-}C_{12}$ and $C_2N/n\text{-}C_{14}$ denote ratios of C_2 alkylbenzenes/C_9 *n*-alkane, C_3 alkylbenzenes/C_{10} *n*-alkane, naphthalene/C_{12} *n*-alkane and C_2 alkylnaphthalene/C_{14} *n*-alkane, respectively. The $C_2B/n\text{-}C_9$ and $C_3B/n\text{-}C_{10}$ ratios of the initial sample, i.e. whole rock extracts and expelled oil, were not obtained due to the loss of these compounds in the Soxhlet extraction and rotary evaporation (see Fig. 3). The $C_2N/n\text{-}C_{14}$ ratio of initial values in the KO series were not calculated due to the very low abundances of C_2 alkylnaphthalenes.

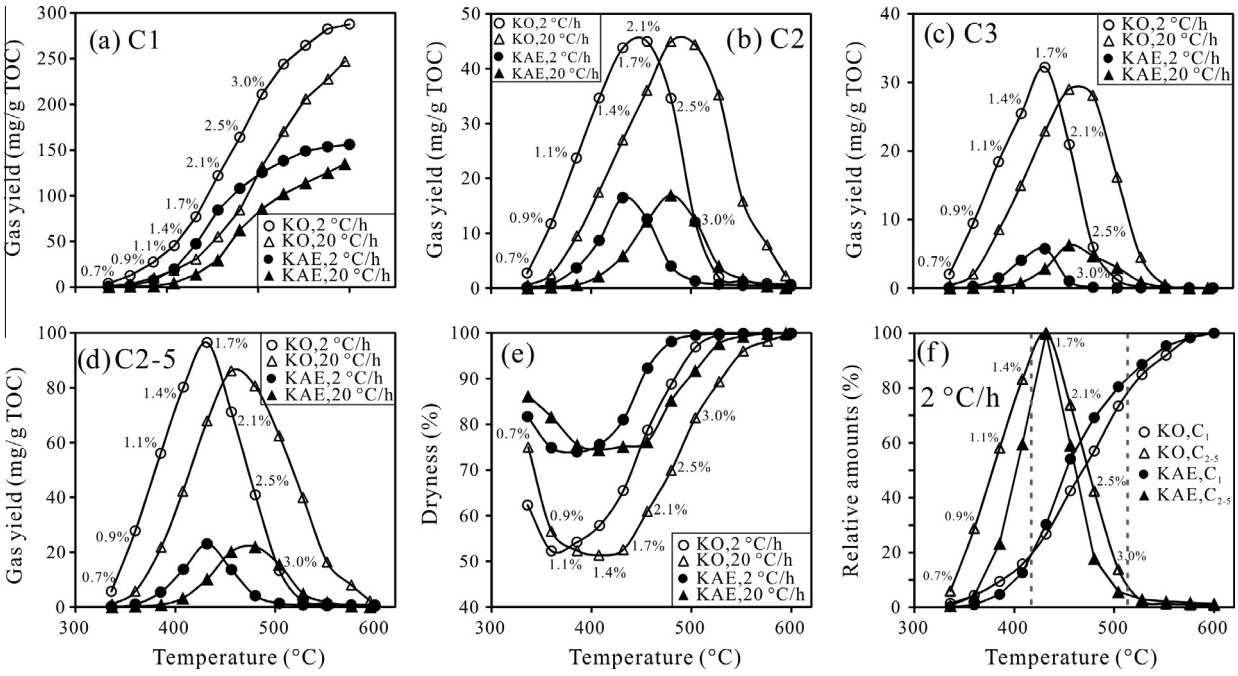

Fig. 5. Gas yields from the pyrolysis of KO and KAE at various temperatures. Dryness was calculated by molar ratios of C_1/C_{1-5}. The relative amounts are normalized to the yields at the temperatures of 600 °C and 432 °C for methane and C_{2-5}, respectively.

of residual bitumens largely contributed to the gases generated by KAE. In the second stage, methane generation from the KAE was slightly faster than that from the KO, suggesting that the oil cracking may occur in relatively higher maturity stages than the cracking of kerogen. The relative amounts of C_{2-5} hydrocarbons generated by KO were much higher than those generated by KAE in the first and second stages at the same maturity level, indicating that the oil is more easily cracked into wet gas components than the kerogen itself.

Behar et al. (1997) reported an interesting result in which the methane production from extracted mature kerogen of type I/II/IIs lies in a very narrow range (47–59 mg/g kerogen), and Lorant and Behar (2002) considered this methane fraction as the late methane generated by mature kerogen alone. Table 1 lists the maximal yields of methane from mature or highly mature kerogen samples measured in closed system. Clearly, the methane yields generated by highly mature kerogen (1.3–1.4%Ro; Behar et al., 1995; Lorant and Behar, 2002) were only one third to one half of those generated by mature kerogen samples (1.0–1.2%Ro). Moreover, it was calculated that methane generated by secondary cracking still contributed 10–20% to the total methane yields even for the two highly mature kerogen samples, and methane yields directly from the type II/III kerogen cracking were ~65 mg/g TOC (Lorant and Behar, 2002). Assuming a methane yield directly from type II kerogen of 58 mg/g TOC, an arbitrary average value of 50 mg/g TOC reported by Behar et al. (1995) and 65 mg/g TOC by Lorant and Behar (2002), the secondary cracking of residual bitumens could contribute ~62.6% of the total methane yield

Table 1
Maximal methane yields of mature kerogens.

Type	Ro (%)	Yield (mg/g TOC)	Sample	References
II	~1.4	50	Artificial maturation	Behar et al. (1995)
II	1.4	~70	Nature sample	Lorant and Behar (2002)
III	1.3	~81	Nature sample	Lorant and Behar (2002)
II	1.15	~115	Nature sample	Hill et al. (2007)
I	1.17	~160	Artificial maturation	Guo et al. (2009)
II	1.1	~160	Nature sample	Tian et al. (2010)
II	1.0	155	Artificial maturation	This work

(155 mg/g TOC, Table 1) from the KAE in this work. The retention of bitumen in kerogen or in source rock seems to be important for conventional and unconventional gas occurring at the high maturity stage even for samples whose expulsion efficiency reaches 58%.

3.1.4. Kinetic modeling of gas generation

Hydrocarbon generation of complicated organic matter, such as kerogen and oil, is a function of time and temperature (Tissot and Welte, 1984). It could involve multiple order reactions, but for convenience in exploration, the generation process was usually simplified and described as multiple parallel first order reactions (Ungerer et al., 1988; Behar et al., 1992; Horsfield et al., 1992; Schenk et al., 1997; Waples, 2000). Non-isothermal experimental data were mostly used to produce the distribution of activation energies and model the complicated hydrocarbon generation from the decomposition of kerogen or oil. In the present study, kinetic parameters of the generation of methane and total gases from the two kerogen samples (KO and KAE) were determined using the software Kinetics developed by Braun and Burnham. Due to the compensation effect between the activation energies and the frequency factor (Waples, 2000), a fixed frequency factor was used in the kinetic modeling for the comparison of gas generation process between sample KO and KAE. We followed the methods used by Hill et al. (2007), and the sum of total errors between experimental data and calculated results was obtained when the frequency factor was adjusted between $1 \times 10^{12}\ s^{-1}$ and $1 \times 10^{18}\ s^{-1}$. In most cases, relatively low values of the sum of error squares for methane generation (0.25–0.30) and total gas generation (0.3–0.4) were observed when the frequency factor was fixed at $1 \times 10^{12}\ s^{-1}$ and $1 \times 10^{13}\ s^{-1}$. For convenience, a frequency factor of $1 \times 10^{13}\ s^{-1}$ was finally applied in the kinetic modeling, and the obtained results for the gas generation of KO and KAE are shown in Fig. 6a–l. Using these activation energies and frequency factor, the conversion and yield of methane or total gas from the kerogen KO and KAE were determined (2 °C/h, Fig. 6m–r) and EasyRo values were also modeled according to the method reported by Sweeney and Burnham (1990).

Although the activation energies for the methane generation from both KO and KAE mainly range from 55–70 kcal/mol, the percentage of relatively low activation energies (55–60 kcal/mol) for methane generation from KAE was much higher than that for methane from KO (Fig. 6a and b), which might be related to higher conversion of methane from KAE compared with that from KO in the main stage of methane generation (Fig. 5f). The generation of methane and total gas from kerogen KAE generally showed a narrow range of activation energies compared with that from kerogen KO (Fig. 6c–f). Such phenomena could be ascribed to the oil expulsion of kerogen KAE.

The generation curves of total gas in weight show notable differences from those of total gas in volume (Fig. 6i–l), which has been well reported by previous studies (Pan et al., 2010, 2012; Tian et al., 2012). The generation curve of total gas mainly reflected the primary cracking of oil (C_{6+}) into gas, while the generation curve of total gas in volume could be used to demonstrate the secondary cracking of wet gas components (C_{2-5}) into methane (Pan et al., 2010). As a result, higher conversion and slightly lower activation energies of total gas in weight (Fig. 6c and i) could be observed relative to those of total gas in volume (Fig. 6e and k). The conversion rate of methane (Fig. 6m) and total gas (in volume, Fig. 6q) for kerogen KAE were lower than those for kerogen KO when EasyRo value < 1.8%. The trend was reversed when EasyRo value was > 1.8%. The difference of yield of methane or total gas in volume between KAE and KO were more pronounced at the high maturity stage. As seen in Fig. 6n and 6r, in EasyRo range from 1.8–3.0%, the yield of methane and total gas in volume from the pyrolysis of kerogen KAE were 30–45% and 40–45% less than those from the pyrolysis of kerogen KO. In the meantime, the yield of total gas in weight from the pyrolysis of kerogen KAE were 50–45% less than those from the pyrolysis of kerogen KO. Again, these results demonstrate that oil expulsion and retention are important factors that should be taken into account in gas reserve evaluation in deep-burial basins.

3.2. Carbon isotopic compositions of residual solids and generated hydrocarbons

Generally, the thermogenic hydrocarbon generation of type I/II kerogen could be divided into those produced in the oil generation stage (0.6–1.35%Ro), condensate and wet gas stage (1.35–2.0%Ro) and dry gas stage (Ro > 2.0%; Tissot and Welte, 1984; Schimmelmann et al., 2006 and references therein). Considering this general classification and the experimental data for residual solids, liquid hydrocarbons and gas hydrocarbons in this study (Figs. 1–5), the evolution of the type II Pingliang kerogen could be divided into three stages (Fig. 7): (1) the main generation stage of oil and oil co-generated gas from kerogen (EasyRo value 0.7–1.1%); (2) the main cracking stage of oil (EasyRo value 1.1–1.7%), corresponding to the condensate or wet gas stage; and (3) cracking of wet gas hydrocarbons (EasyRo value 1.7–3.0%). However, there is overlap between these three stages, due to the co-existing primary and secondary generation of hydrocarbons in the simulation experiments in closed and open systems (Behar et al., 1997; Dieckmann et al., 2000).

3.2.1. $\delta^{13}C$ values of residual solids

Carbon isotopic compositions of residual solids after pyrolysis showed slight but definite differences between KO and KAE as maturation progressed (2 °C/h, Fig. 7). At pyrolysis temperatures < 500 °C, which were equivalent to the oil generation and wet gas cracking stages, $\delta^{13}C$ values of the residual solids of KAE showed a limited increment of ~0.2‰ while the residual solids of KO became progressively enriched in ^{13}C by up to ~0.7‰. Moreover, the residual solids of KO were enriched in ^{13}C by ~0.5‰ at pyrolysis temperatures < 400 °C (oil generation stage) and there was little fluctuation in $\delta^{13}C$ values between 400 °C and 500 °C (the oil cracking and wet gas cracking stages). At pyrolysis temperatures higher than 500 °C, there was little difference in carbon isotopic compositions between the residual solids of KO and of KAE. In the oil generation stage, progressive ^{13}C enrichment in the residual solids of KO could be explained by the preferential release of oil that are relatively enriched in ^{12}C due to the kinetic isotopic fractionation in the pyrolysis (Clayton, 1991). This explanation is also supported by the greater ^{13}C enrichment of KAE than that of KO in this stage (Fig. 7).

In the oil and wet gas cracking stages, progressive ^{13}C enrichment of kerogens stops but about 0.2–0.3‰ enrichment of ^{13}C was still observed in the residual solids of KAE when compared

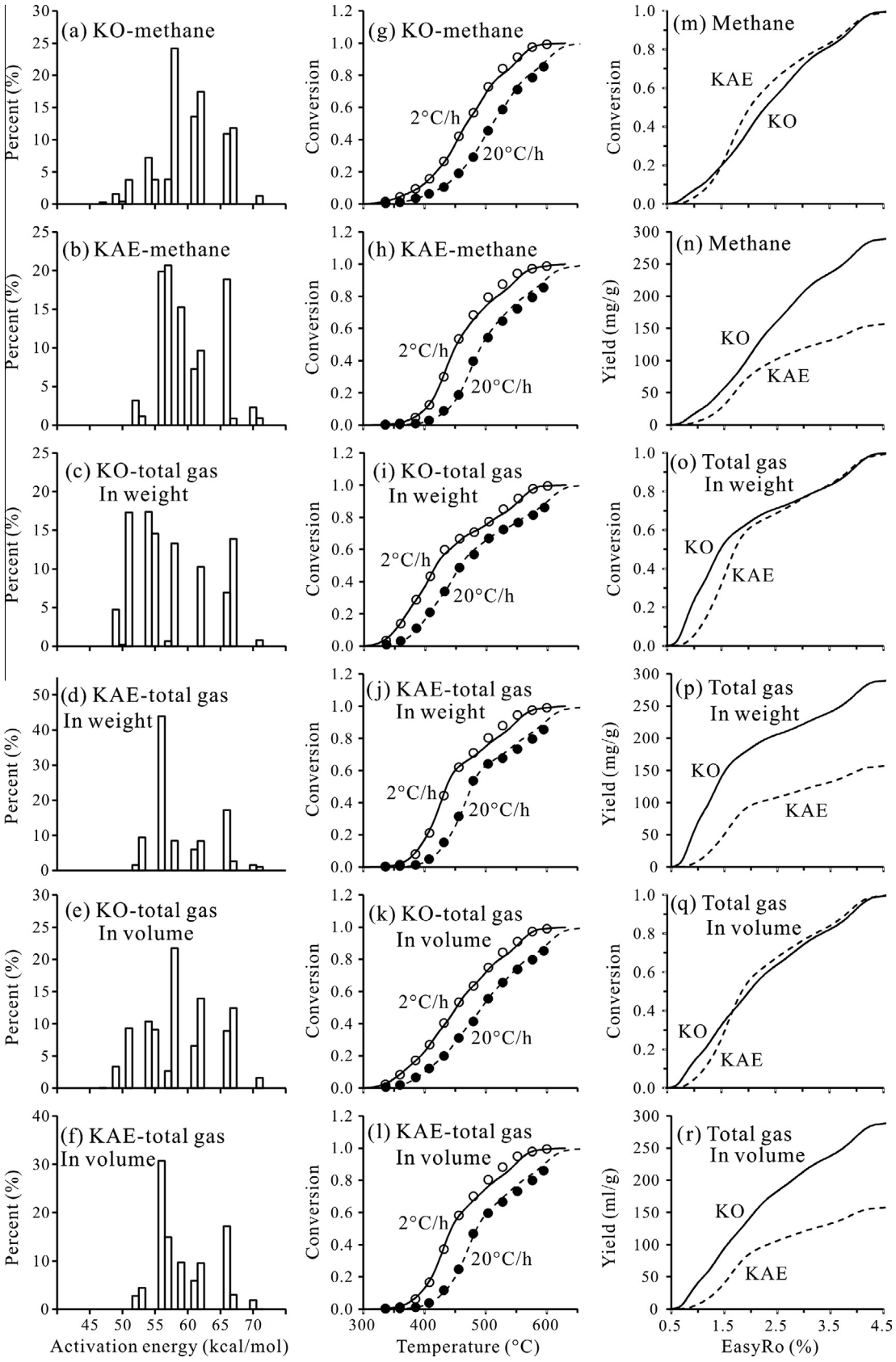

Fig. 6. The distribution of activation energies (a–f) and fitting curves (g–l) for the generation of methane and total gas obtained for the experimental data. Fig. 6m–r show variations of calculated conversion and yield of methane or total gas with EasyRo values at 2 °C/h.

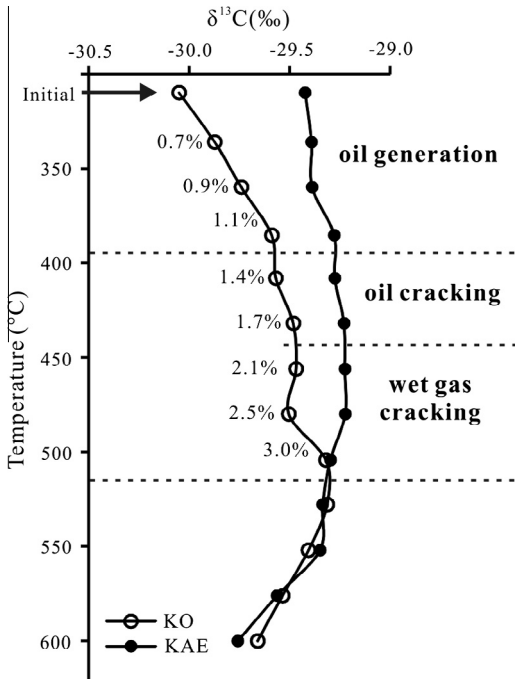

Fig. 7. Carbon isotopic compositions of the residual solids of two kerogen samples at different pyrolysis temperatures (2 °C/h).

with those of KO (Fig. 7). This result might be explained by the end of oil generation and heavier $\delta^{13}C$ values of KAE.

Notably, the reversed isotopic trends in residual solids of two kerogens after heating to 500 °C and higher (Fig. 6) were observed. We interpret this phenomenon to be the formation of pyrobitumen and addition of pyrobitumen to kerogens. Pyrobitumen could be formed after the main oil generation stage and might be depleted in ^{13}C relative to the kerogen because it is mainly derived from the cracking of generated oils. Addition of pyrobitumen will cause lighter $\delta^{13}C$ values of kerogen. However, this argument needs confirmation of further experiments.

The variation in $\delta^{13}C$ values of the residual solids of two kerogens across all the experiments was < 0.8‰. Limited variations in $\delta^{13}C$ values of kerogens have been well documented by both simulation experiments and analysis of natural rock samples (Lewan, 1983; Buchard et al., 1986; Clayton, 1991). Lewan (1983) observed ~0.5‰ enrichment in ^{13}C of type II kerogen in the hydrous pyrolysis performed in a closed system, while > 1‰ enrichment in ^{13}C was displayed by one kerogen sample in the pyrolysis performed in open system (Clayton, 1991). It is reasonable that the oil expulsion could affect $\delta^{13}C$ values of the residual kerogen during the pyrolysis.

3.2.2. $\delta^{13}C$ and δD values of n-alkanes in liquid pyrolysates

n-Alkanes generated from KO became progressively enriched in ^{13}C with increasing pyrolysis temperatures (oil generation stage, Fig. 8a), which agrees well with the increasing amounts of *n*-alkanes released by the kerogen under enhanced thermal stress (Fig. 2). There was a sharp increase of $\delta^{13}C$ in *n*-alkanes when the pyrolysis temperature increased from 384 °C to 408 °C (Fig. 8a), which could be related to secondary cracking of *n*-alkanes as indicated by the decreasing amounts of *n*-alkanes in the pyrolysates (Fig. 2). In the pyrolysis of an oil sample in a closed system, significant enrichments in ^{13}C and D were observed in *n*-alkanes when the EasyRo values were higher than 1.1% (Tang et al., 2005). Bjorøy et al. (1992) documented similar results in the hydrous pyrolysis of a shale sample containing type II kerogen, and the *n*-alkanes with longer chains were more enriched in ^{13}C relative to those with short chains. However, no significant variations in $\delta^{13}C$ values of *n*-alkanes of different carbon numbers were observed in our experiments with type II kerogen. The hydrous pyrolysis of different types of source rocks suggested that *n*-alkanes of different carbon numbers released during maturation could exhibit complicated variations with respect to their ^{13}C contents (Bjorøy et al., 1992).

At pyrolysis temperatures below 384 °C, the $\delta^{13}C$ values of *n*-alkanes in the pyrolysates of KAE were nearly the same (Fig. 8b), which suggesting that *n*-alkanes generated from KAE are identical in $\delta^{13}C$ or undergo very little degradation at relatively low temperatures. Moreover, carbon isotopic compositions of *n*-alkanes were the same as those in the expelled oil, suggesting there was no significant carbon isotopic fractionation during the oil expulsion. When the pyrolysis temperature increased from 384 °C to 408 °C, *n*-alkanes in the pyrolysates of KAE also exhibited a sharp increase in their $\delta^{13}C$ values, and the amounts of *n*-alkanes in the pyrolysates decreased concomitantly (Fig. 2). Although there were no isotopic differences between *n*-alkanes in expelled oil and those in residual bitumens (Fig. 8b), it is interesting to observe that *n*-alkanes in the pyrolysates of KAE at 384 °C and 408 °C were more enriched in ^{13}C, by ~1‰, relative to those in the pyrolysates of KO.

Variations in hydrogen isotopes of *n*-alkanes released from KO and KAE in the pyrolysis show notable differences from those of the carbon isotopes (Fig. 9). *n*-Alkanes released by KO and KAE at 360 °C were slightly more enriched in D relative to those generated at 336 °C, by ~10‰, while no further enrichments in D could be observed for *n*-alkanes generated at 384 °C compared with those generated at 360 °C (Fig. 9). This result is slightly different from the progressive enrichments in ^{13}C of *n*-alkanes in this temperature range (Fig. 8a). A possible explanation is that pyrolysis of kerogen in oil the window is mostly involved in carbon rather than hydrogen in kerogen. Indeed, only cleavage of carbon–carbon bonds will lead to oil formation from kerogen. When the pyrolysis temperature was elevated from 384 °C to 408 °C (corresponding to the EasyRo value range from 1.1% to 1.4%), significant enrichments in D, by ~20‰, were clearly observed for the *n*-alkanes possibly due to bond cleavages already associated with hydrogen. Overall, *n*-alkanes generated by the kerogen samples could be enriched in D by 40–50‰ in the maturation process. Tang et al. (2005) observed that δD values of *n*-alkanes increased rapidly when the EasyRo value increased from 1.1% to 1.5% during oil cracking in a closed system, consistent with the results reported in this work. There were few variations in δD values of *n*-alkanes with the EasyRo values ranging from 0.9% to 1.1%, but a rapid increase of δD (by 50‰) during the oil cracking process (Tang et al., 2005). D enrichments in *n*-alkanes, by 30–40‰, have also been reported for natural oil samples at various maturity stages (Li et al., 2001; Jia et al., 2013). However, *n*-alkanes in extracts from natural sediments and rocks might display more complicated variations in hydrogen isotopes during maturation, although a general trend of D enrichment for *n*-alkanes has been observed (Dawson et al., 2005, 2007; Radke et al., 2005; Pedentchouk et al., 2006; Schimmelmann et al., 2006; Kikuchi et al., 2010). This is due to the diversity of sources of *n*-alkanes in sediments and rocks, and in some cases hydrogen exchange with inorganic hydrogen either in water or minerals has taken place. In the pyrolysis experiments under anhydrous conditions, those variations are well controlled and δD values of *n*-alkanes display more clear variations under increasing thermal stress.

Fig. 9 also indicates that *n*-alkanes generated by KAE were more strongly enriched in D, by ~20‰, relative to those generated by KO at the same pyrolysis temperatures (384 °C and 408 °C, Fig. 9). However, the *n*-alkanes generated by KAE only displayed ~1‰

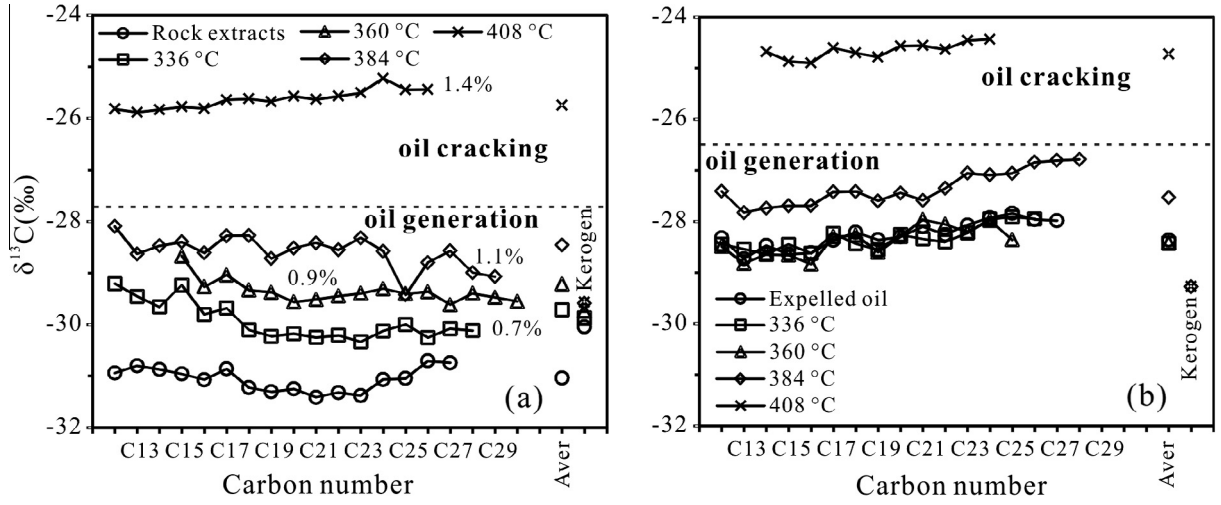

Fig. 8. Carbon isotopic compositions of *n*-alkanes released from KO (a) and KAE (b) at different pyrolysis temperatures (2 °C/h). The expelled oil in Fig. 8b refers to extracts from the sand when the KAE samples were prepared (see Section 2.2.1). The label 'Aver' denotes weighted mean $\delta^{13}C$ value of *n*-alkanes, calculated by summing the measured delta values of individual *n*-alkanes multiplied by their percentage weights as determined by GC analysis.

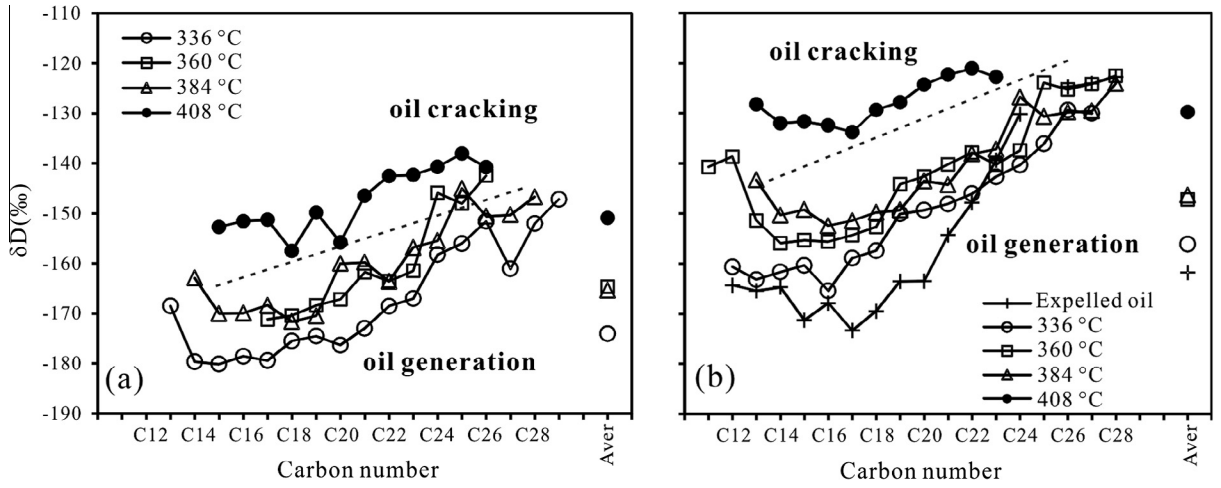

Fig. 9. Hydrogen isotopic compositions of *n*-alkanes released by KO (a) and KAE (b) at different pyrolysis temperatures (2 °C/h). The label 'Aver' denotes weighted mean δD value of *n*-alkanes, calculated by summing the measured delta values of individual *n*-alkane multiplied by their percentage weights as determined by GC analysis.

additional enrichment in ^{13}C relative to those generated by KO (Fig. 8). Oil expulsion had more pronounced effects on the hydrogen isotopes than carbon isotopes in *n*-alkanes generated in high maturity stage due to the relatively strong isotopic fractionations of D and H caused by the much larger mass difference between H and D (Tang et al., 2005).

Enrichment in both D and ^{13}C in *n*-alkanes generated by KAE relative to KO suggests that oil expulsion does affect isotopic compositions of *n*-alkanes produced in high maturation. The possible explanation for this is that *n*-alkanes relatively depleted in D or ^{13}C are preferentially released from the kerogen structure in the main oil generation stage (Clayton, 1991; Tang et al., 2000). The oil expulsion causes those *n*-alkanes to leave the kerogen and the residual kerogen is therefore enriched in D and ^{13}C. At the high maturity stage, the newly formed *n*-alkanes are isotopicaly heavier since they are derived from residual kerogen. In contrast, *n*-alkanes from KO are more depleted in D and ^{13}C due to the lack of oil expulsion and also the greater contribution of *n*-alkanes from the secondary cracking of oil which are produced in the main oil generation stage.

3.2.3. $\delta^{13}C$ values of gas hydrocarbons

In the oil generation stage, $\delta^{13}C$ values of methane generated from both KO and KAE decreased with elevated pyrolysis temperatures, and it is notable that methane from KAE displayed relatively smaller variations in $\delta^{13}C$ values compared with methane from KO (Fig. 10). Initial enrichment in ^{12}C for methane under enhanced thermal stress during pyrolysis might suggest multiple precursors for methane (Tang et al., 2000). In the oil cracking and wet gas cracking stages, methane generated from the two kerogen samples is progressively enriched in ^{13}C as pyrolysis temperature increases. For ethane and propane, the $\delta^{13}C$ values increase slowly with increasing temperature in the oil generation stage and early stage of oil cracking and start to increase rapidly in the late stage of oil cracking and the wet gas cracking stage. The oil expulsion effects, e.g. the leaving of oil with lighter $\delta^{13}C$ value, on the carbon isotopic compositions of gases generated in high to overmature stages were very pronounced (Fig. 10), and the mass loss of kerogen by oil expulsion must have influenced $\delta^{13}C$ values. The $\delta^{13}C$ values of methane, ethane and propane generated by KAE were higher than those generated by

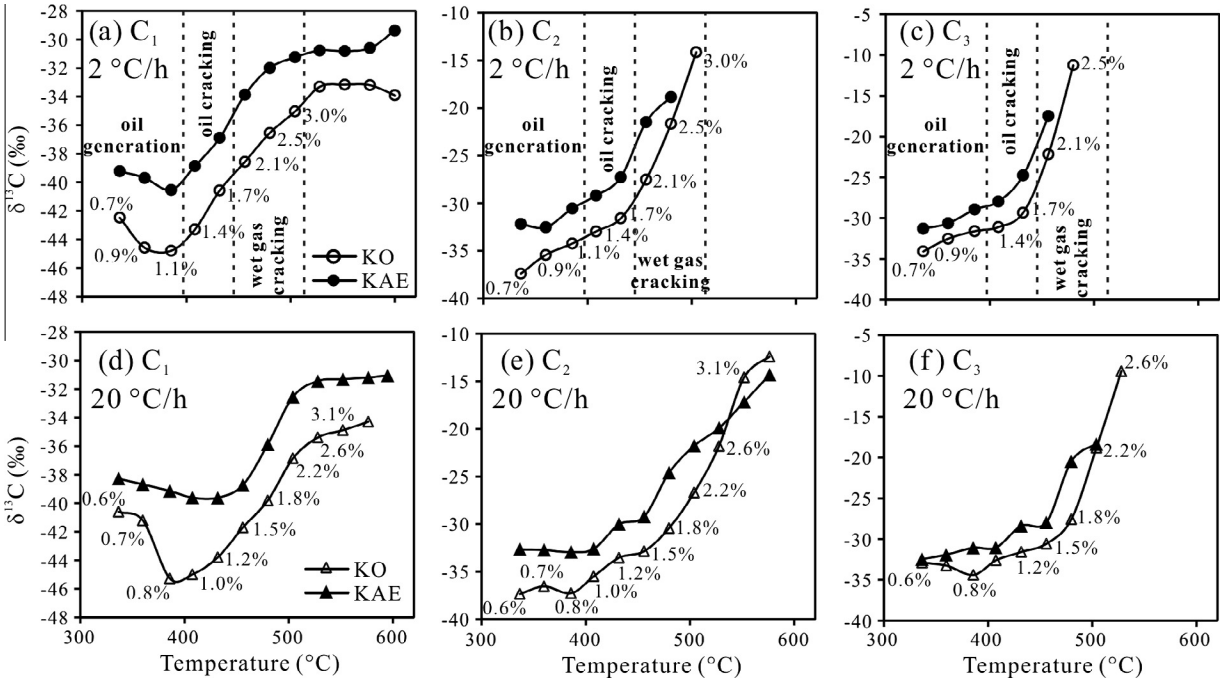

Fig. 10. Carbon isotopic compositions of C_{1-3} gas hydrocarbons generated by KO and KAE at different pyrolysis temperatures.

KO, by 4–6‰. Nevertheless, variations in $\delta^{13}C$ values of gases generated by KAE and KO show similar trends (Fig. 10), which could suggest that the differences in $\delta^{13}C$ values between gases generated by KAE and by KO are mainly related to $\delta^{13}C$ values of precursors for the gases in the two kerogens.

The large difference in the $\delta^{13}C$ values of methane from KAE and KO suggest that gas–gas or source–gas correlation performed for kerogen II in deep-burial basins should consider expulsion efficiency of source rock.

3.3. Oil expulsion or retention effects revealed by crossplots of $\delta^{13}C_2$–$\delta^{13}C_3$ versus C_2/C_3, $\delta^{13}C_2$–$\delta^{13}C_3$ versus $\delta^{13}C_1$ and $\delta^{13}C_1$–$\delta^{13}C_2$ versus $\ln(C_1/C_2)$

It has long been noted that crossplots displaying volumetric proportions of ethane/propane versus the difference of $\delta^{13}C$ values between ethane and propane, are useful for distinguishing gases derived from kerogen cracking or from oil cracking (Prinzhofer and Huc, 1995). Lorant et al. (1998) further concluded that these crossplots could illustrate the openness and maturity of the source rock bed from which the gases were generated. Gas generation experiments with coal, performed in a stepwise, semi-open system, strongly supported this conclusion (Michels et al., 2002). Recent thermal simulations further show that this type of crossplot combined with two other crossplots, specifically $\delta^{13}C_2$–$\delta^{13}C_3$ versus $\delta^{13}C_1$ and $\delta^{13}C_1$–$\delta^{13}C_2$ versus C_1/C_2, may differentiate gases generated by kerogen cracking from those generated by oil cracking (Guo et al., 2009; Tian et al., 2010). Although residual bitumens were the main contributors to gas generated in KAE, as stated above, the gases generated from KAE displayed very similar characteristics to those reported from mature kerogens (Guo et al., 2009; Tian et al., 2010) and coal in semi-open systems (Michels et al., 2002) on the $\delta^{13}C_2$–$\delta^{13}C_3$ versus C_2/C_3 crossplot (Fig. 11a). Moreover, gases generated from KO exhibited similar trends to those from coal in closed systems (Lorant et al., 1998; Michels et al., 2002), and were also close to gases generated from two oils in a closed system (Guo et al., 2009; Tian et al., 2010). In summary, the effect of oil expulsion or retention on a source rock's position within a crossplot of $\delta^{13}C_2$–$\delta^{13}C_3$ versus C_2/C_3 suggests the expulsion or retention process constrains whether the extent of how open or close the system was. The source itself has little influence on this crossplot, as suggested by Lorant et al. (1998).

On the crossplot $\delta^{13}C_2$–$\delta^{13}C_3$ versus $\delta^{13}C_1$ (Fig. 11b), the gases generated by KAE are very similar to those reported for type I mature kerogen in a closed system (Guo et al., 2009), while gases from KO are similar to those reported for low maturity kerogen samples (Lorant et al., 1998; Tian et al., 2010) and oils in closed systems (Guo et al., 2009). However, gases generated by a mature kerogen (Tian et al., 2010) show different characteristics to those reported for a mature kerogen sample by Guo et al. (2009) and for KAE in this work and gases generated by cracking of two oil samples (Guo et al., 2009; Tian et al., 2010) are also highly distinct from each other. The oil expulsion or retention could indicate the extent to which the system was open may influence the source rock's position in the $\delta^{13}C_2$–$\delta^{13}C_3$ versus $\delta^{13}C_1$ crossplot. It also seems that source also influences the data trend in a $\delta^{13}C_2$–$\delta^{13}C_3$ versus $\delta^{13}C_1$ crossplot.

In the crossplot of $\delta^{13}C_1$-$\delta^{13}C_2$ versus $\ln(C_1/C_2)$, the gases generated from KO and KAE display distinct evolutionary trends (Fig. 11c). However, the gases from low maturity kerogen samples, e.g. those reported by Lorant et al. (1998) and this work, are slightly different. The gases generated from mature kerogen samples are also inconsistent with each other (Guo et al., 2009; this work). Similar to the $\delta^{13}C_2$–$\delta^{13}C_3$ versus $\delta^{13}C_1$ crossplot, the sources, maturity and openness (closeness) of the source rock bed determine the pattern of data in the $\delta^{13}C_1$–$\delta^{13}C_2$ versus $\ln(C_1/C_2)$ crossplot. The oil expulsion or retention still indicate the extent of openness of the source bed, influencing the positions of data points on the $\delta^{13}C_1$–$\delta^{13}C_2$ versus $\ln(C_1/C_2)$ crossplot.

As discussed above, oil expulsion or retention may affect data patterns in all three plots, each of which is commonly used to identify the genesis of gases. The understanding of oil expulsion or retention behavior in these three plots may constrain the applicability of the plots in gas geochemistry. We constructed the additional crossplot $\delta^{13}C_1$–$\delta^{13}C_3$ versus $\ln(C_1/C_3)$ in Fig. S3, which may also differentiate the gases generated by oil-expelled kerogen from those generated by fresh kerogen.

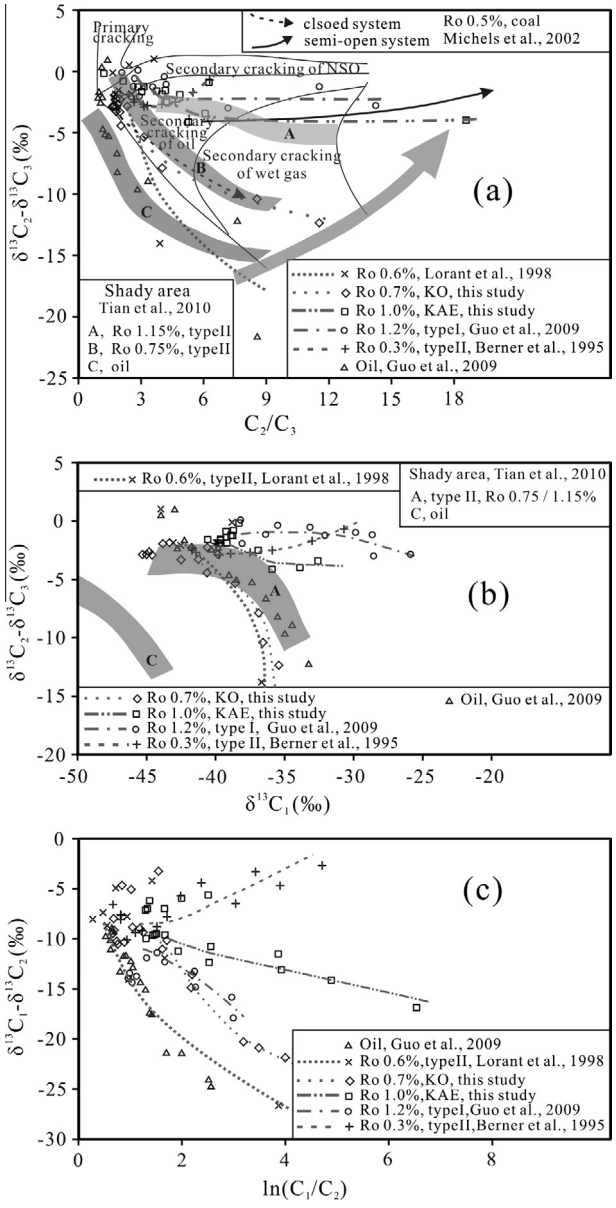

Fig. 11. Crossplot of (a) $\delta^{13}C_2-\delta^{13}C_3$ versus C_2/C_3 (after Lorant et al. (1998), Guo et al. (2009) and Tian et al. (2010)), (b) $\delta^{13}C_2-\delta^{13}C_3$ versus $\delta^{13}C_1$ (after Guo et al. (2009) and Tian et al. (2010)) and (c) $\delta^{13}C_1-\delta^{13}C_2$ versus $\ln(C_1/C_2)$ (after Guo et al. (2009)) for gases generated by kerogens and oils in this work and previous studies. Data from Berner et al. (1995) were obtained in open system.

4. Conclusions

A comparative study of the pyrolysis of type II kerogens before and after oil expulsion yields the following conclusions.

Oil expulsion or retention strongly affects the amount of subsequent oil and gas generation at the high maturity stage. As exemplified by this study, gas production will reduce by 50% if the expulsion coefficient reaches 58% and gases generated by oil-expelled kerogen are much drier than those generated by fresh kerogen. Conventional and unconventional reserve estimation in deep-burial basins must consider oil expulsion efficiency, or retention ability of source rock.

Oil expulsion will cause kerogen, oil and gas at the highly mature stage to have heavier carbon isotopic compositions. The additional enrichments of ^{13}C in *n*-alkanes and gas hydrocarbons are 1.0‰ and 4–6‰, respectively. The effect of oil expulsion should be considered in the context of gas isotopic compositions in gas–gas or source–gas correlation in deep-burial basins.

Oil expulsion controls the extent to which a system is open versus closed and influences the data pattern in crossplots of $\delta^{13}C_2-\delta^{13}C_3$ versus C_2/C_3, $\delta^{13}C_2-\delta^{13}C_3$ versus $\delta^{13}C_1$ and $\delta^{13}C_1-\delta^{13}C_2$ versus $\ln(C_1/C_2)$. This suggests that oil expulsion or retention is another important factor that should be considered when those plots are used to identify the genesis of gases.

Acknowledgments

This work was supported by National Oil and Gas Major Project (2011ZX05008-002), China National Fundamental Research Program (2012CB214704) and Natural Science Foundation of China (41073038). We are grateful to two anonymous reviewers for their critical comments that significantly improved the quality of manuscript. The authors also thank Prof. Lloyd R. Snowdon and Dr. Andrew Murray for handling of this paper. This is contribution No. IS-1862 from GIGCAS.

Appendix A. Supplementary material

Supplementary data associated with this article can be found, in the online version, at http://dx.doi.org/10.1016/j.orggeochem.2014.03.009.

Associate Editor—**Andrew Murray**

References

Andresen, B., Throndsen, T., Råheim, A., Bolstad, J., 1995. A comparison of pyrolysis products with models for natural gas generation. Chemical Geology 126, 261–280.
Behar, F., Kressman, S., Rudkiewicz, J.L., Vandenbroucke, M., 1992. Experimental simulation in a confined system and kinetic modeling of kerogen and oil cracking. Organic Geochemistry 19, 173–189.
Behar, F., Vandenbroucke, M., Teermann, S.C., Hatcher, P.G., Leblond, C., Lerat, O., 1995. Experimental simulation of gas generation from coals and a marine kerogen. Chemical Geology 126, 247–260.
Behar, F., Vandenbroucke, M., Tang, Y., Marquis, F., Espitalié, J., 1997. Thermal cracking of kerogen in open and closed systems: determination of kinetic parameters and stoichiometric coefficients for oil and gas generation. Organic Geochemistry 26, 321–339.
Behar, F., Budzinski, H., Vandenbroucke, M., Tang, Y., 1999. Methane generation from oil cracking: kinetics of 9-methylphenanthrene cracking and comparison with other pure compounds and oil fractions. Energy & Fuel 13, 471–481.
Berner, U., Faber, E., Scheeder, G., Panten, D., 1995. Primary cracking of algal and landplant kerogens: kinetic models of isotope variations in methane, ethane and propane. Chemical Geology 126, 233–245.
Bjorøy, M., Hall, K., Hustad, E., Williams, J.A., 1992. Variation in the stable carbon isotope ratios of individual hydrocarbons as a function of artificial maturity. Organic Geochemistry 19, 89–105.
Buchard, B., Clausen, J., Thomsen, E., 1986. Carbon isotope composition of Lower Paleozoic kerogen: effects of maturation. Organic Geochemistry 10, 127–134.
Carrigan, W.J., Jones, P.J., Tobey, M.H., Halpern, H.I., Wender, L.E., Philp, R.P., Allen, J., 1998. Geochemical variations among eastern Saudi Arabian Paleozoic condensates related to different source kitchen areas. Organic Geochemistry 29, 785–798.
Chen, J.H., Fu, J.M., Sheng, G.Y., Liu, D.H., Zhang, J.J., 1996. Diamondoid hydrocarbon ratios: novel maturity indices for highly mature crude oils. Organic Geochemistry 25, 179–190.
Clayton, C.J., 1991. Effect of maturity on carbon isotopic ratios of oils and condensates. Organic Geochemistry 17, 887–899.
Dawson, D., Grice, K., Alexander, R., 2005. Effect of maturation on the indigenous δD signatures of individual hydrocarbons in sediments and crude oils from the Perth Basin (Western Australia). Organic Geochemistry 36, 95–104.
Dawson, D., Grice, K., Alexander, R., Edwards, D., 2007. The effect of source and maturity on the stable isotopic compositions of individual hydrocarbons in sediments and crude oils from the Vulcan Sub-basin, Timor Sea, Northern Australia. Organic Geochemistry 38, 1015–1038.
Dieckmann, V., Schenk, H.J., Horsfield, B., Welte, D.H., 1998. Kinetics of petroleum generation and cracking by programmed-temperature closed-system pyrolysis of Toarcian shales. Fuel 77, 23–31.
Dieckmann, V., Schenk, H.J., Horsfield, B., 2000. Assessing the overlap of primary and secondary reactions by closed- versus open-system pyrolysis of marine kerogens. Journal of Analytical and Applied Pyrolysis 56, 33–46.

Ertas, D., Kelemen, S.R., Halsey, T.C., 2006. Petroleum expulsion Part 1. Theory of kerogen swelling in multicomponent solvents. Energy & Fuels 20, 295–300.
Eseme, E., Littke, R., Krooss, B.M., Schwarzbauer, J., 2007. Experimental investigation of the compositional variation of petroleum during primary migration. Organic Geochemistry 38, 1373–1397.
Fekete, J., Sajgó, C., Demény, A., 2009. Hydrogen isotope type-curves of very hot crude oils. Rapid Communication of Mass Spectrometry 25, 191–198.
Guo, L.G., Xiao, X.M., Tian, H., Song, Z.G., 2009. Distinguishing gases derived from oil cracking and kerogen maturation: insights from laboratory pyrolysis experiments. Organic Geochemistry 40, 1074–1084.
Hao, F., Zou, H.Y., 2013. Cause of shale gas geochemical anomalies and mechanisms for gas enrichment and depletion in high-maturity shales. Marine and Petroleum Geology 44, 1–12.
Hao, F., Li, S.T., Su, Y.C., Zhang, Q.M., 1996. Characteristics and origin of the gas and condensate in the Yinggehai basin, offshore South China Sea: evidence for effects of overpressure on petroleum generation and migration. Organic Geochemistry 24, 363–375.
Hill, R.J., Tang, Y.Y., Kaplan, I.R., 2003. Insights into oil cracking based on laboratory experiments. Organic Geochemistry 34, 1651–1672.
Hill, R.J., Zhang, E.T., Katz, B.J., Tang, Y.C., 2007. Modeling of gas generation from the Barnett Shale, Fort Worth Basin, Texas. American Association of Petroleum Geologists Bulletin 91, 501–521.
Horsfield, B., Schenk, H.J., Mills, N., Welte, D.H., 1992. Closed-system programmed-temperature pyrolysis for simulating the conversion of oil to gas in a deep petroleum reservoir. Organic Geochemistry 19, 191–204.
Jia, W.L., Wang, Q.L., Peng, P.A., Xiao, Z.Y., Li, B.H., 2013. Isotopic compositions and biomarkers in crude oils from the Tarim Basin: oil maturity and oil mixing. Organic Geochemistry 57, 95–106.
Kelemen, S.R., Walters, C.C., Ertas, D., Freund, H., Curry, D.J., 2006a. Petroleum expulsion Part 3. A model of chemically driven fractionation during expulsion of petroleum from kerogen. Energy & Fuels 20, 309–319.
Kelemen, S.R., Walters, C.C., Ertas, D., Kwiatek, L.M., Curry, D.J., 2006b. Petroleum expulsion Part 2. Organic matter type and maturity effects on kerogen swelling by solvents and thermodynamic parameters for kerogen from regular solution theory. Energy & Fuels 20, 301–308.
Kikuchi, T., Suzuki, N., Saito, H., 2010. Change in hydrogen isotope composition of *n*-alkanes, pristane, phytane, and aromatic hydrocarbons in Miocene siliceous mudstones with increasing maturity. Organic Geochemistry 41, 940–946.
Lewan, M.D., 1983. Effects of thermal maturation on stable organic carbon isotopes as determined by hydrous pyrolysis of Woodford Shale. Geochimica et Cosmochimica Acta 47, 1471–1479.
Lewan, M.D., 1997. Experiments on the role of water in petroleum formation. Geochimica et Cosmochimica Acta 61, 3691–3723.
Lewan, M.D., Roy, S., 2011. Role of water in hydrocarbon generation from Type-I kerogen in Mahogany oil shale of the Green River Formation. Organic Geochemistry 42, 31–41.
Leythaeuser, D., Radke, M., Wilsch, H., 1988. Geochemical effects of primary migration of petroleum in Kimmeridge source rocks from Brae field area, North Sea. II: Molecular composition of alkylated naphthalenes, phenanthrenes, benzo- and dibenzothiophenes. Geochimica et Cosmochimica Acta 52, 2879–2891.
Li, M., Huang, Y., Obermajer, M., Jiang, C., Snowdon, L.R., Fowler, M.G., 2001. Hydrogen isotopic compositions of individual alkanes as a new approach to petroleum correlation: case studies from the Western Canada Sedimentary Basin. Organic Geochemistry 32, 1387–1399.
Liu, J.Z., Tang, Y.C., 1998. Kinetics of early methane generation from Green River shale. Chinese Science Bulletin 43, 1908–1912.
Lorant, F., Behar, F., 2002. Late generation of methane from mature kerogens. Energy & Fuels 16, 412–427.
Lorant, F., Prinzhofer, A., Behar, F., Huc, A.Y., 1998. Carbon isotopic and molecular constraints on the formation and the expulsion of thermogenic hydrocarbon gases. Chemical Geology 147, 249–264.
Lorant, F., Behar, F., Vandenbroucke, M., 2000. Methane generation from methylated aromatics: kinetic study and carbon isotope modeling. Energy & Fuels 14, 1143–1155.
Michels, R., Enjelvin-Raoult, N., Marcel, E., Mansuy, L., Faure, P., Oudin, J.L., 2002. Understanding of reservoir gas compositions in a natural case using stepwise semi-open artificial maturation. Marine and Petroleum Geology 19, 589–599.
Pan, C.C., Yu, L.P., Liu, J.Z., Fu, J.M., 2006. Chemical and carbon isotopic fractionations of gaseous hydrocarbons during abiogenic oxidation. Earth Planet Science Letters 246, 70–89.
Pan, C.C., Jiang, L.L., Liu, J.Z., Zhang, S.C., Zhu, G.Y., 2010. The effects of calcite and montmorillonite on oil cracking in confined pyrolysis experiments. Organic Geochemistry 41, 611–626.
Pan, C.C., Jiang, L.L., Liu, J.Z., Zhang, S.C., Zhu, G.Y., 2012. The effects of pyrobitumen on oil cracking in confined pyrolysis experiments. Organic Geochemistry 45, 29–47.
Pang, X.Q., Li, M.W., Li, S.M., Jin, Z.J., 2005. Geochemistry of petroleum systems in the Niuzhuang South Slope of Bohai Bay Basin: Part 3. Estimating hydrocarbon expulsion from the Shahejie Formation. Organic Geochemistry 36, 497–510.
Pedentchouk, N., Freeman, K.H., Harris, N.B., 2006. Different response of δD values of *n*-alkanes, isoprenoids, and kerogen during thermal maturation. Geochimica et Cosmochimica Acta 70, 2063–2072.
Pepper, A.S., Corvi, P.J., 1995. Simple kinetic models of petroleum formation. Part III: Modelling an open system. Marine and Petroleum Geology 12, 417–452.
Prinzhofer, A.A., Huc, A.Y., 1995. Genetic and post-genetic molecular and isotopic fractionations in natural gases. Chemical Geology 126, 181–190.
Radke, M., Welte, D.H., 1983. The methylphenanthrene index (MPI): a maturity parameter based on aromatic hydrocarbons. In: Bjorøy, M., Albrecht, P., Cornford, C., de Groot, K., Eglinton, G., Galimov, E., Leythaeuser, D., Pelet, R., Rullkötter, J., Speers, G. (Eds.), Advances in Organic Geochemistry 1981. Wiley, Chichester, UK, pp. 504–512.
Radke, J., Bechtel, A., Gaupp, R., Püttmann, W., Schwark, L., Sachse, D., Gleixner, G., 2005. Correlation between hydrogen isotope ratios of lipid biomarkers and sediment maturity. Geochimica et Cosmochimica Acta 69, 5517–5530.
Ritter, U., 2003. Solubility of petroleum compounds in kerogen: implications for petroleum expulsion. Organic Geochemistry 34, 319–326.
Rodriguez, N.D., Philp, R.P., 2010. Geochemical characterization of gases from the Mississippian Barnett Shale, Fort Worth Basin, Texas. American Association of Petroleum Geologists Bulletin 94, 1641–1656.
Sajgó, C., 2000. Assessment of generation temperatures of crude oils. Organic Geochemistry 31, 1301–1323.
Sandvik, E.I., Young, W.A., Curry, D.J., 1992. Expulsion from hydrocarbon sources: the role of organic adsorption. Organic Geochemistry 19, 77–87.
Schenk, H.J., di Primio, R., Horsfield, B., 1997. The conversion of oil into gas in petroleum reservoirs. Part 1: Comparative kinetic investigation of gas generation from crude oils of lacustrine, marine and fluviodeltaic origin by programmed-temperature closed-system pyrolysis. Organic Geochemistry 26, 467–481.
Schimmelmann, A., Lewan, M.D., Wintsch, R.P., 1999. D/H isotope ratios of kerogen, bitumen, oil, and water in hydrous pyrolysis of source rocks containing kerogen types I, II, IIS, and III. Geochimica et Cosmochimica Acta 63, 3751–3766.
Schimmelmann, A., Sessions, A.L., Mastalerz, M., 2006. Hydrogen isotopic (D/H) composition of organic matter during diagenesis and thermal maturation. Annual Review of Earth and Planetary Sciences 34, 501–533.
Stahl, W.L., 1978. Source rock-crude oil correlation by isotopic type-curves. Geochimica et Cosmochimica Acta 42, 1573–1577.
Sweeney, J.J., Burnham, A.K., 1990. Evaluation of a simple model of vitrinite reflectance based on chemical kinetics. American Association of Petroleum Geologists Bulletin 74, 1559–1570.
Tang, Y.C., Perry, J.K., Jenden, P.D., Schoell, M., 2000. Mathematical modeling of stable carbon isotope ratios in natural gases. Geochimica et Cosmochimica Acta 64, 2673–2687.
Tang, Y.C., Huang, Y., Ellis, G.S., Wang, Y., Kralert, P.G., Gillaizeau, B., Ma, Q.S., Hwang, R., 2005. Kinetic model for thermally induced hydrogen and carbon isotope fractionation of individual *n*-alkanes in crude oil. Geochimica et Cosmochimica Acta 69, 4505–4520.
Thomas, M.M., Clouse, J.A., 1990. Primary migration by diffusion through kerogen: II. Hydrocarbon diffusivities in kerogen. Geochimica et Cosmochimica Acta 54, 2775–2779.
Tian, H., Xiao, X.M., Wilkins, R.W.T., Gan, H.J., Guo, L.G., Yang, L.G., 2010. Genetic origins of marine gases in the Tazhong area of the Tarim Basin, NW China: implications from the pyrolysis of marine kerogens and crude oil. International Journal of Coal Geology 82, 17–26.
Tian, H., Xiao, X.M., Wilkins, R.W.T., Tang, Y.C., 2012. An experimental comparison of gas generation from three oil fractions: implications for the chemical and stable carbon isotopic signatures of oil cracking gas. Organic Geochemistry 46, 96–112.
Tissot, B.P., Welte, D.H., 1984. Petroleum Formation and Occurrence, second ed. Springer-Verlag, Berlin.
Ungerer, P., Behar, F., Villalba, M., Heum, O.R., Audibert, A., 1988. Kinetic modelling of oil cracking. Organic Geochemistry 13, 857–868.
Walters, C.C., Freund, H., Kelemen, S.R., Peczak, P., Curry, D.J., 2007. Predicting oil and gas compositional yields via chemical structure–chemical yield modeling (CS–CYM): Part 2 – Application under laboratory and geologic conditions. Organic Geochemistry 38, 306–322.
Waples, D.W., 2000. The kinetics of in-reservoir oil destruction and gas formation: constraints from experimental and empirical data, and from thermodynamics. Organic Geochemistry 31, 553–575.
Wei, Z.F., Zou, Y.R., Cai, Y.L., Wang, L., Luo, X.R., Peng, P.A., 2012. Kinetics of oil group-type generation and expulsion: an integrated application to Dongying Depression, Bohai Bay Basin, China. Organic Geochemistry 52, 1–12.
Xia, X.Y., Chen, J., Braun, R., Tang, Y.C., 2013. Isotopic reversals with respect to maturity trends due to mixing of primary and secondary products in source rocks. Chemical Geology 339, 205–212.
Xiong, Y.Q., Geng, A.S., Wang, Y.P., Liu, D.H., Jia, R.F., Shen, J.G., Xiao, X.M., 2002. Kinetic simulating experiment on the secondary hydrocarbon generation of kerogen. Science in China Series D 45, 13–20.
Zhang, S.C., Huang, H.P., Xiao, Z.Y., Liang, D.G., 2005. Geochemistry of Palaeozoic marine petroleum from the Tarim Basin, NW China. Part 2: Maturity assessment. Organic Geochemistry 36, 1215–1225.
Zhang, W.Z., Yang, H., Li, J.F., Ma, J., 2006. Leading effect of high-class source rock of Chang 7 in Ordos Basin on enrichment of low permeability oil-gas accumulation—hydrocarbon generation and expulsion mechanism. Petroleum Exploration & Development 33, 289–293 (in Chinese with English abstract).
Zhou, Y., Sheng, G.Y., Fu, J.M., Geng, A.S., Chen, J.H., Xiong, Y.Q., Zhang, Q.M., 2003. Triterpane and sterane biomarkers in the YA13-1 condensates from Qiongdongnan Basin, South China Sea. Chemical Geology 199, 343–359.